Energy hierarchies governing quarkonium dynamics in heavy ion collisions

Rishi Sharma* and Balbeer Singh†
Tata Institute of Fundamental Research Colaba, Mumbai 400005, India

(Received 24 May 2023; revised 12 January 2024; accepted 10 April 2024; published 8 May 2024)

In this paper, we critically examine hierarchies between the energy scales that determine quarkonium dynamics in the quark gluon plasma. A particularly important role is played by the ratio of the binding energy of species (E_b) and the medium scales; temperature (T) and Debye mass (m_D). It is well known that if these ratios are much larger than 1 then the dominant process governing quarkonium evolution is dissociation by thermal gluons (gluodissociation). On the other hand, if the ratio E_b/T is much smaller than one then quarkonium dynamics is dominated by screening and Landau damping of the exchanged gluons. Here we show that over most of the evolution, the scale hierarchies do not fall in either limit and one needs to use the full structure of the gluonic spectral function to follow the dynamics of the $Q\bar{Q}$ pair. This has a significant bearing when we follow the quantum dynamics of quarkonia in the medium. The inverse medium relaxation time is also $\approx T$ and if E_b is comparable (or larger) in magnitude to T, the quantum evolution of $Q\bar{Q}$ is nonlocal in time within the Brownian approximation.

DOI: 10.1103/PhysRevC.109.054905

I. INTRODUCTION

In the vacuum, the bound states of heavy quarks (Q, which can be b or c) and antiquarks ($\bar{Q}$) feature three prominent momentum scales: the heavy quark masses M, the inverse relative separation $\frac{1}{r}$, and the binding energies E_b (see Ref. [1] for a comprehensive review). These scales satisfy the hierarchies $M \gg \frac{1}{r} \gg E_b$, which justifies nonrelativistic treatments of these states. An additional relevant scale for their description is the scale of quantum chromodynamics ($\Lambda_{\rm QCD}$), which may or may not be somewhat smaller than E_b [1] but can be assumed to be significantly smaller than $1/r$ (especially for $\bar{b}b$ pair). The hierarchy of these scales allows one to integrate out modes at the scale M, and $1/r$ systematically, and derive a low-energy effective field theory (EFT) valid at the scale E_b. At the lowest order in rE_b, the EFT consists of nonrelativistic quarks bound by a potential [2]. At higher order, the theory features interactions mediated by gluons of wavelength $1/E_b$. Effects of higher-order terms are suppressed by positive powers of rE_b, where factors of r can be seen as arising from a long wavelength expansion of the fields. This framework is called pNRQCD [1].

In a thermal medium at temperature T, new scales appear, which govern the dynamic properties of quarkonia in the medium. It was pointed out in a classic paper [3] that the screening of the $Q\bar{Q}$ interaction on an inverse length scale m_D could lead to the melting of the bound states. Moreover, later on, it was realized that scattering between bound states and the thermal constituents of the medium plays a major role in the dissociation of the quarkonium states. This leads to the generation of the imaginary part of the quarkonium potential in a thermal medium [4]. Additionally, absorption of thermal gluons in the medium could lead to gluodissociation [5]. It was shown [6] that pNRQCD naturally incorporates processes leading to gluodissociation [5,7] as its dynamical degree of freedom that includes low-energy gluonic degrees of freedom (and other light degrees of freedom if any) in addition to the wave functions of $Q\bar{Q}$ pair. The corresponding emergent scale $\Gamma \approx 1/\tau_R$ (where τ_R is the relaxation time of quarkonia) is related to the dynamics of inelastic interactions of $\bar{Q}Q$ with the medium. Furthermore, E_b and $1/r$ might themselves be modified from their vacuum values by these thermal effects.

Two medium scales that play a role in quarkonium dynamics in the quark gluon plasma (QGP) are T and m_D. In the weak-coupling limit, there is a hierarchy between m_D and T [8]. In this regime, the coupling g is small and $m_D \approx gT \ll T$. However, for the temperatures of interest (150–500 MeV), lattice results suggest that $m_D/T \approx 2$ [9]. Using $2\pi T$ as the relevant energy scale [10] at which α_s is computed, also gives similar values of g.

This implies that in this regime, leading-order, weak-coupling expressions in g are not quantitatively reliable. For example, it is known that the higher-order corrections to the momentum diffusion coefficient are larger than the leading-order value [11]. However, nonperturbative calculations of some relevant dynamical processes are still challenging and weak-coupling calculations are still useful. An important result in weak coupling was obtained in Ref. [4], which showed

*rishi.sharma@gmail.com
†balbeer@theory.tifr.res.in

Published by the American Physical Society under the terms of the Creative Commons Attribution 4.0 International license. Further distribution of this work must maintain attribution to the author(s) and the published article's title, journal citation, and DOI. Funded by SCOAP³.

that the potential between quark-antiquark pair is complex at finite T. Recently, in the weak-coupling limit, the qualitative effects (for Υ states) of the finite-energy difference between singlet and octet state has also been investigated in Ref. [12]. It was observed that these corrections lead to a reduction in the decay width when compared to the imaginary potential. (For more details see Refs. [13,14].) In an alternate approach to include the effects of the finite-energy difference of singlet and octet state, one can make an E_b/T expansion in the Lindblad operators to obtain a Lindblad equation and keep higher-order terms in E_b/T. Up to NLO this has been implemented in Ref. [15] in pNRQCD. Such weak-coupling calculations have given insight into the problem and results from these calculations can be used to obtain estimates for experimental observables of interest: for example R_{AA} in heavy ion collisions (HIC).

Many such calculations have been attempted to address the phenomenology of quarkonium states in the QGP (see Ref. [16] for a review). For approaches using a medium-modified T-matrix approach see Refs. [17–23]. Gluodissociation as the dominant mechanism for dissociation has been used in Refs. [24–26]. For approaches based on the complex potentials derived by Ref. [4] see Refs. [27–32]. For approaches based on Schrödinger-Langevin equation see Refs. [33–35]. Quarkonia at high p_T have been explored in Refs. [36–38]. For quantum dynamics in weak coupling see Refs. [39–43].

In this paper, we will focus on bottomonia and use leading-order expressions for the gluon polarization tensor. But we will not assume that m_D/T is small. This is not a formal expansion in g but might better capture some important qualitative dynamical properties of the QGP. This has been used in other papers for open heavy flavor [44].

The next question is how the thermal scales compare to the scales associated with bound states. Clearly, $M \gg T$ and a nonrelativistic treatment is applicable for quarkonia slowly moving in the medium. For bottomonia, the values of $1/r$ are comparable to $\approx$1 GeV [45] and we will assume that $1/r \gg T$ and hence use pNRQCD to describe the system. However, we do not assume that the hierarchy between $1/r$ and the screening mass m_D is so strong that we can ignore the screening of the $Q\bar{Q}$ potential when calculating quarkonium properties in the medium. In practice, we see that the effect of screening on the Υ(1S) wave function is small, but the Υ(2S) and Υ(3S) states are affected by screening.

On the other hand, there is no clear separation between E_b and m_D, T (see Fig. 4). Moreover, their relative order depends on the species and can change as the medium cools down as it evolves. In this paper, we will take all three to be of the same order. Therefore, a nonrelativistic treatment is still applicable. However, the integration of modes from $1/r$ to E_b includes thermal effects.

Here we would like to point out that further assuming scale separations between E_b, m_D, and T can allow us to write simpler EFTs assuming specific choices of these hierarchies. These have been investigated in detail in a series of papers [6,46–48]. Our goal in this paper is to avoid assuming a clear separation between the three scales. In specific regimes where the separations exist, our results will clearly reduce to results from Refs. [46,48]. However, we will see that in a wide range of parameters, physics lies in an intermediate regime where clear separations do not exist.

To do this we use the full perturbative form of the gluon spectral function. We include contributions from the transverse and longitudinal gluons both in the Landau damping (LD) regime and in the spacelike regime where gluodissociation occurs. This gives a clear framework to include both processes in a unified language and allows us to compare the contributions to decay from the various process. This is the first time the full gluonic spectral function applicable in both kinematic regimes has been used to compute the total decay rates. In our calculation, the singlet wave function is approximated to be the instantaneous eigenstate of a lattice inspired thermal potential and hence incorporates screening. For the octet state, the spectrum is fixed by the constraint that at large r the real part of the octet potential approaches the real part of the singlet potential. For the wave function, we systematically compare two limiting cases: one where the screening is strong that the potential is flat in r and the other where the screening is very weak. These can be seen as limiting cases of the physical situation where the screening length is comparable to that in the singlet channel [49].

The comparison between E_b and T is shown in Fig. 4, which clarifies that these two scales are close to each other. The consequence of this is shown in Fig. 7 where we show for the Υ(1S) state gluodissociation dominates in a wide temperature region of interest. Figure 8 shows that for the Υ(2S) state also both contributions are comparable. Finally, we find that (Fig. 6) the imaginary potential overpredicts the contribution from LD substantially.

The plan of the paper is as follows. In Sec. II we will review the formalism and highlight the assumptions and approximations involved in our method. In Sec. III, we discuss the connection between EE correlator and the momentum diffusion coefficient of heavy quark, particularly, in the static limit. In Sec. IV, we discuss the implementation of the real part of the singlet potential to obtain the singlet wave function at a given T. We also discuss the two extreme cases of complete screening and no screening for octet interactions. Finally, in Sec. V, we discuss our results followed by the conclusion and future directions in Sec. VI.

II. FORMALISM

pNRQCD [1] is an EFT for bound states of quarkonia. In vacuum, it relies on the hierarchy of scales $M \gg \frac{1}{r} \gg E_b$. The scale separation $M \gg \frac{1}{r}$ ensures that the Q and $\bar{Q}$ are nonrelativistic, and $\frac{1}{r} \gg E_b$ means that the interactions between Q and $\bar{Q}$ (at leading order in $1/M$) can be written as potentials.

One can think of it as a two-step process where relativistic dynamics of Q and $\bar{Q}$ are integrated out first, to obtain NRQCD at scales $1/r$ [50]. If $1/r \gg T, m_D$, the energies corresponding to the thermal scales is much smaller than the relative momentum between $Q\bar{Q}$ ($\approx 1/r$) then NRQCD at this scale is unaffected by T, m_D, and hence this theory is the same as the theory in vacuum [50].

The pNRQCD Lagrangian is obtained by integrating out modes from $1/r$ to E_b. The structure of the EFT is governed only by the symmetries and the particle content of the theory. In the rest frame of $Q\bar{Q}$ in vacuum, this theory has been extensively studied [1].

While the medium introduces a new vector u^μ associated with the medium rest frame, which can lead to additional operators in the Lagrangian [51], we only consider the case where the quarkonium is (nearly) at rest in the medium, and hence the form of the Lagrangian is unchanged from that in vacuum. The Lagrangian is of the form [1]

$$\begin{aligned}\mathcal{L} = \mathrm{tr}\Bigg\{ & S^\dagger\left(i\partial_t + \frac{\nabla^2}{M} - V_s(r)\right)S \\ & + O^\dagger\left(i\partial_t + \frac{\nabla^2}{M} - V_o(r)\right)O \\ & + gV_A(r)[S^\dagger r\cdot E O + O^\dagger r\cdot E S] \\ & + g\frac{V_B(r)}{2}[O^\dagger r\cdot E O + O^\dagger O r\cdot E]\Bigg\} + \cdots . \end{aligned} \tag{1}$$

Here $S(O)$ is the singlet (octet) wave function in the relative coordinate between Q and $\bar{Q}$. $V_s(V_o)$ is the $Q\bar{Q}$ potential in the singlet (octet) channel. $M/2$ is the reduced mass. The dots correspond to terms that are higher order in the (nonrelativistic) relative speed between Q and $\bar{Q}$.

The Lagrangian [Eq. (1)] is obtained by systematically performing a multipole expansion which encodes the factorization of wavelengths of the order of $1/E_b$ compared to the short distance r. The dots represent higher-order terms in this expansion.

The low-energy coefficients (LEC's) $V_A(r)$, $V_B(r)$ are 1 at leading order in perturbation theory and are expected to be close to 1 at a short distance. In our paper, we will take them to be 1. The other input to the theory are the potentials, $V_s(r)$ and $V_o(r)$. If $E_b \sim T, m_D$, then the integration of modes from $1/r$ to E_b is affected by the medium and hence the functional forms of $V_s(r)$ and $V_o(r)$ is different from their forms in vacuum. If the Q and $\bar{Q}$ can be treated as static (for example if their mass is so high that their kinetic energy can be ignored), then one can run the integration of modes all the way to zero energy. It is well known that in this limit V_s and V_o are complex [4,6]. The real and imaginary parts of the static potentials have been calculated in weak-coupling limit [4,6,52]. Moreover, we also expect that nonperturbative contributions to the potential are substantial especially for the excited states of bottomonia, because while $1/r$ is large compared to Λ_{QCD} the hierarchy is not very strong. Additionally, neither E_b nor T are much larger than Λ_{QCD} and hence the medium itself at this scale is strongly coupled. Both the real and imaginary parts of V_s [53–57] and V_o [49] have been computed nonperturbatively on the lattice.

Let us note that a complex potential describes the $Q\bar{Q}$ dynamics under the assumption that E_b is the smallest scale in the problem and the kinetic energies of the Q and $\bar{Q}$ are negligible. However, if E_b and T are comparable, one needs to go beyond the static approximation. In this case the thermal losses can not be captured by an imaginary potential.

The potential at the scale E_b to leading order in the $1/M$ expansion is given by the static limit of the gluon exchange diagram (in weak coupling) or the long-time behavior of the Wilson loop (nonperturbatively). It picks up an imaginary piece from dynamics at scales $\sim T$ if $T \gg E_b$. However, if $T \sim E_b$ (or if $E_b > T$) then the imaginary part is small [46,48].

Formally, assuming the hierarchy $1/r \gg T \sim E_b \sim m_D$ in pNRQCD, the real part of the potential at the scale E_b is the vacuum potential [46,48]. This is the Coulombic potential to the lowest order in α_s. This is one of the cases we consider below.[1]

However, the scale m_D can be larger than T. For example, estimates of the screening length on the lattice [9,58] give values of m_D roughly twice of T. In such cases it is plausible that screening effects in the medium operate on a shorter scale than T. Furthermore, one can incorporate the long-distance part of the potential and its screening by adding a screened Cornell component. This sort of a potential is not formally needed for $1/r \gg T \sim E_b \sim m_D$, if one remains within the validity regime of pNRQCD since pNRQCD is valid in the limit where $1/r \gg \Lambda_{\mathrm{QCD}}, T$. However, such potentials have been widely considered in phenomenology (e.g., Refs. [18,20,31]) by taking the real part of the potential from the lattice [49,54,56,57,59–61]. For $\Upsilon(1S)$ the results from the Coulombic and the nonperturbative potentials do not differ significantly. However, the excited states are wider, and the long-distance parts of the potential do affect results. By considering both, we therefore explore systematics associated with the choice of the potentials, even though the use of nonperturbative potentials is not completely self-consistent within pNRQCD with our hierarchy.

On the other hand, to estimate losses due to thermal process, we compute the imaginary part of the singlet self-energy diagram in the multipole expansion. The key assumption here is that in the pNRQCD Lagrangian [Eq. (1)] at scale $\approx E_b$, the imaginary part of the potential is small and losses predominantly arise from dynamics at scales $\approx E_b$. In this hierarchy it is important to take into account finite frequency effects in the gluon spectral function to calculate decay rate.

Finite frequency corrections also appear in the real part of the self-energy. These corrections can change the energy of the singlet as well as the octet states and hence change the binding energy of the bound states. These also change the eigenstates of the singlet and octet Hamiltonians. However, the effect of this contribution on the decay rate of the singlet state is higher order in the multipole expansion (r^4 instead of r^2) and can be safely ignored in our calculation.

Finally, we assume that the octet state, once formed, decoheres rapidly and can no longer lead to a reformation of the singlet state. In quantum calculations [40,43,62] these processes can be taken into account but this is beyond the scope of our paper.

[1]While tracking the quantum dynamics of quarkonia, other medium scales also play a role. For example, the time scales of medium dynamics have been argued to be $\approx 1/(\pi T)$ [10]. This will not play a role in the rate-equation approach we follow here.

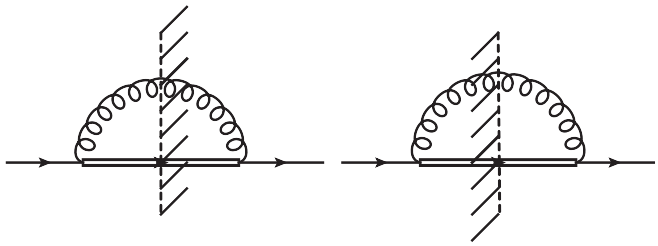

FIG. 1. Cut diagrams contributing to the decay width. Single solid line is for singlet and double lines for octet. The gluon line corresponds to a dressed gluon.

With this setup, let us start from a singlet state. The dissociation is given by the imaginary part of the singlet self-energy correction. The corresponding diagram is shown in Fig. 1. Here, the gluon line is resummed and gets contributions both from LD, which arises from the imaginary part of the gluon self-energy and pole of the gluon propagator. In Fig. 1, gluon momentum (k_0, k) is directed inward at the first vertex and octet momentum (q_0, q) is directed outward from the same vertex. The incoming momentum of the singlet is $p_\mu = q_\mu - k_\mu$.

In order to calculate the imaginary part of the singlet self-energy, we follow the cutting rules at the finite temperature are given in Refs. [63,64]. There are two cut diagrams as shown in Fig. 1. Following the cut rules and implementing appropriate propagator for each cut diagram, the imaginary part of the self-energy reads as

$$\begin{aligned}\Im\Sigma_{11}(p_0,p,r) = \frac{g^2C_F}{6} r_i\Bigg(\int \frac{d^4k}{(2\pi)^4}\Big\{&\rho_o\theta(q_0)(\theta(-k_0)\\ &+ f(|k_0|))\big[k_0^2\rho_{jj}(k_0,k) + k_j^2\rho_{00}(k_0,k)\big]\Big\}\\ &+ \int \frac{d^4k}{(2\pi)^4}\big\{\rho_o\theta(-q_0)(\theta(k_0) + f(|k_0|))\\ &\times\big[k_0^2\rho_{jj}(k_0,k) + k_j^2\rho_{00}(k_0,k)\big]\big\}\Bigg) r_i. \end{aligned} \tag{2}$$

To avoid this lengthy expression, from here onwards we use the following shorthand notation for the above equation:

$$\Im\Sigma_{11}(p_0,p,r) = r_i\hat{\mathcal{O}}(p_0,p,r)r_i. \tag{3}$$

In Eq. (2), C_F $(= 4/3)$ is color factor. $\rho_{00}(k_0,k)$ and $\rho_{jj}(k_0,k)$ are gluon spectral functions that are discussed in the next section. $p_\mu = (p_0, \mathbf{0})$ is the four-momentum of the incoming singlet state, and ρ_o is the tree level $Q\bar{Q}$ spectral function in the octet channel, which can be obtained from the octet propagator [see Eq. (1)]

$$G(q_0) = \frac{1}{q_0 - \nabla^2/M - V_o}. \tag{4}$$

Hence,

$$\begin{aligned}&\rho_o = 2\pi\delta(k_0 + p_0 - \hat{q}_0), \quad \text{where}\\ &\hat{q}_0 = V_o + \frac{\nabla^2}{M}. \end{aligned} \tag{5}$$

To proceed further we need information about the temporal and spatial gluonic spectral functions, ρ_{00} and ρ_{ii}, which we discuss below.

A. Gluon-polarization tensor

In this section, we review the well-known expressions for the gluon polarization tensor [65] that are essential inputs to the evaluation of the imaginary part of quarkonium self-energy. The general form of the gluon self-energy is given as

$$\Pi_{\mu\nu}(k_0,k) = P^L_{\mu\nu}\Pi_L(k_0,k) + P^T_{\mu\nu}\Pi_T(k_0,k), \tag{6}$$

where $P^L_{\mu\nu}(P^T_{\mu\nu})$ are longitudinal (transverse) projection operators and $\Pi_L(\Pi_T)$ are component of the gluon self-energy along these directions. In order to evaluate quarkonium decay width using Eq. (3), we need the imaginary part of the gluon propagator. This may come from the pole of the propagator in the region of phase space where the imaginary part of the gluon self-energy is zero, and from the region where the imaginary part of the gluon self-energy is finite. The pole contribution is nonvanishing in the limit $k_0 > k$, and the latter contribution that requires the real and imaginary parts of the gluon self-energy is finite when $k_0 < k$ [65]. Below we discuss various components of the gluon self-energy.

Let us first consider the regime $k_0 < k$ (spacelike). This we call the Landau damping regime. The gluon loop contribution to the imaginary part of the longitudinal component of the gluon self-energy is given as

$$\begin{aligned}\Im\Pi^g_L(k_0,k) = \frac{g^2N}{4\pi k}\int_{\frac{k+k_0}{2}}^{\infty} dq\, q^2\left(2 + \frac{k^4}{4q^4} - \frac{k^2}{q^2}\right)\\ \times[f(q-k_0) - f(q)]\,\theta(k-k_0), \end{aligned} \tag{7}$$

where $N = 3$ and $f(q)$ is Bose-Einstein distribution function. Let us note that with an expansion in k_0/T in the distribution function and by taking the limit $k \ll q$, Eq. (7) goes to its hard thermal loop (HTL) counterpart.

Similarly, The quark loop contribution with N_f (light) quark flavors to the imaginary part of the longitudinal component of the gluon self-energy is given as

$$\begin{aligned}\Im\Pi^f_L(k_0,k) = \frac{g^2N_f}{2\pi k}\int dq\left(q^2 - \frac{k^2}{4}\right)[\tilde{f}(q-k_0)\\ - \tilde{f}(q)]\,\theta(k-k_0), \end{aligned} \tag{8}$$

where $\tilde{f}(q)$ is Fermi-Dirac distribution function. The total imaginary part of the longitudinal gluon self-energy can be obtained by summing Eqs. (7) and (8).

The real part of the longitudinal component of the self-energy is

$$\Re\Pi_L(k_0,k) = m_D^2\left(1 - \frac{k_0}{2k}\log\left|\frac{k+k_0}{k-k_0}\right|\right), \tag{9}$$

where $m_D^2 = \frac{g^2T^2}{3}(N + \frac{N_f}{2})$. In obtaining Eq. (9), we have dropped terms of the order of $k_0/T, k/T$. These terms are important when $k_0, k \gtrsim T$ but we drop these terms because of the following reason. The exact forms of these higher-order terms depend on the gauge (e.g., see Ref. [65]). This is because the

expression is not a formal expansion in g. Moreover Eq. (9) is the HTL form and is gauge invariant [8]. This expression is valid for both $k_0 > k$ and $k_0 < k$. Moreover, from Eq. (3) it is clear that the contribution to $\Im\Sigma$ from $k_0, k \gg T$ is exponentially suppressed and hence making this approximation will not cause a significant error in our result.

Similarly, for the transverse gluon, the imaginary contributions to the gluon self-energy are,

$$\Im\Pi_T^g(k_0,k) = \frac{g^2N}{2\pi k}\int_{\frac{k+k_0}{2}}^{\infty} dq\left[q^2\left(1-\frac{k^2}{2q^2}\right)^2 - \frac{k^2}{4}\right.$$
$$\left.\times\left(2-\frac{k^2}{2q^2}\right)^2\right][f(q-k_0)-f(q)]\theta(k-k_0), \quad (10)$$

and,

$$\Im\Pi_T^f(k_0,k) = \frac{g^2N_f}{8\pi k}\int_{\frac{k+k_0}{2}}^{\infty} dq\left(2q^2+\frac{k^2}{2}\right)$$
$$\times[\tilde{f}(q-k_0)-\tilde{f}(q)]\,\theta(k-k_0). \quad (11)$$

The real part of the transverse component of the gluon self-energy is

$$\Re\Pi_T(k_0,k) = \frac{m_D^2}{2}\left(\frac{k_0^2}{k^2} - \frac{k_0\left(k_0^2-k^2\right)}{2k^3}\log\left|\frac{k+k_0}{k-k_0}\right|\right). \quad (12)$$

Let us now consider the regime $k_0 > k$ (timelike). This we call the pole regime. In this regime, the imaginary part of Π_L and Π_T are zero and the real parts are as above. At order g^3 the widths of these modes are finite [65,66] but we ignore this in our calculation.

Now we can calculate the gluon spectral function, which goes in Eq. (3). Below we discuss it for both timelike and spacelike gluons.

B. Gluon spectral functions

The general form of the gluon spectral function in a medium reads as

$$\rho_{\mu\nu}(k_0,k) = P^L_{\mu\nu}\rho_L(k_0,k) + P^T_{\mu\nu}\rho_T(k_0,k). \quad (13)$$

Here $\rho_L(k_0,k) = D_L^R(k_0,k) - D_L^A(k_0,k)$ is the longitudinal component of the spectral function and $D_L^{R(A)}$ is the longitudinal component of resummed retarded (advanced) gluon propagator. Similarly, one can obtain the transverse component of the spectral function (ρ_T) by using $\rho_T(k_0,k) = D_T^R(k_0,k) - D_T^A(k_0,k)$. Below we discuss the form of these spectral functions for both $k_0 > k$ as well as $k_0 < k$.

For $k_0 < k$ (LD), we use the gluon self-energies (shown in the previous section) to write the resummed gluon propagator and obtain

$$\rho_L(k_0,k) = \frac{2\Im\Pi_L(k_0,k)}{[k^2+\Re\Pi_L(k_0,k)]^2 + [\Im\Pi_L(k_0,k)]^2}, \quad (14)$$

where $\Re\Pi_L(\Im\Pi_L)$ is sum of both gluon and quark contributions.

Similarly, the transverse component of the spectral function can be written as

$$\rho_T(k_0,k) = \frac{2\Im\Pi_T(k_0,k)}{\left[k_0^2-k^2+\Re\Pi_T(k_0,k)\right]^2 + [\Im\Pi_T(k_0,k)]^2}. \quad (15)$$

It is worth mentioning here that the above form of the spectral functions reproduces the momentum diffusion coefficients obtained within the kinetic theory framework in Ref. [44].

For $k_0 > k$ the gluon propagator is simply a pole. The quarkonium dissociation in this regime is due to the absorption of a gluon from thermal medium. This process is known as gluodissociation in the literature. In the limit $k_0 \gg T$, the spectral function is given by the imaginary part of free gluon retarded propagator and gluodissociation in this case has been studied in Refs. [43,47]. However, for realistic situations one needs to take full resummed propagator. Thus, similar to Eq. (13) the general form of the spectral function reads as

$$\rho^p_{\mu\nu}(k_0,k) = \mathcal{P}^L_{\mu\nu}\rho^p_L(k_0,k) + \mathcal{P}^T_{\mu\nu}\rho^p_T(k_0,k), \quad (16)$$

where p stands for pole. The longitudinal spectral function in this regime is given by

$$\rho^p_L(k_0,k) = 2\pi\delta[k^2 - \Re\Pi_L(k_0,k)]. \quad (17)$$

The transverse spectral function is given by

$$\rho^p_T(k_0,k) = 2\pi\delta\left[k_0^2 - k^2 - \Re\Pi_T(k_0,k)\right]. \quad (18)$$

The imaginary part of Σ_{11} gets contribution from both Eqs. (13) and (16). While in the low-frequency limit, LD gives the dominant contribution, pole contributions are significantly large in the intermediate and high-frequency limit. The overall pole contribution merges with their free spectral function counterpart at an asymptotically large frequency. This we show in Fig. 3.

III. CONNECTION WITH THE MOMENTUM DIFFUSION COEFFICIENT

In this section, we relate Eq. (3) with the standard definition of the momentum diffusion coefficient in terms of the electric field correlator, which is given as [67,68]

$$\kappa = \frac{g^2}{3N}\int_{-\infty}^{\infty} dt\,\mathrm{Tr}\langle U(-\infty,t)E_i(t)U(t,0)E_i(0)U(0,-\infty)\rangle, \quad (19)$$

where U is the Wilson line in the fundamental representation, $E_i = \partial_i A_0 - \partial_0 A_i - ig[A_0, A_i]$ is the color electric field and trace over color degrees of freedom. In Eq. (19), the infinite integration limit represents the zero-frequency limit of the correlator. For the leading-order results, one needs to replace the Wilson lines by identity (i.e., $U = \mathbb{1}$) to obtain

$$\kappa = \frac{g^2C_F}{3}\lim_{k_0\to 0}\int d^3k\,k^2\,\langle A_0(k_0,k)A_0(0,0)\rangle$$
$$= \frac{g^2C_F}{3}\lim_{k_0\to 0}\int d^3k\,k^2[1+f(k_0)]\rho_L(k_0,k), \quad (20)$$

for more details see Refs. [44,68,69].

It is useful to compare this quantity [Eq. (20)] to the expression Eq. (3). Imposing the condition $q_0 > 0$ in Eq. (3)

and performing energy integration in Eq. (2) using the energy δ function we rewrite the imaginary part of the singlet self-energy as

$$\Im\Sigma_{11}(k_0) = \frac{g^2 r^2 C_F}{6}\int d^3k f(k_0)\left[k_0^2\rho_{ii}(k_0,k) + k^2\rho_{00}(k_0,k)\right], \tag{21}$$

where $k_0 = p_0 - q_0$. For future use, we define a quantity

$$\tilde{\kappa}(k_0) = \frac{2(\Im\Sigma_{11}(k_0)|_{\rm pole} + \Im\Sigma_{11}(k_0)|_{\rm LD})}{r^2}. \tag{22}$$

A single heavy quark, traversing through the thermal medium, gets uncorrelated random kicks from the medium constituents that give rise to κ. However, for quarkonium bound state, not only scattering but also absorption of thermal gluons contribute to the dissociation. The latter process is kinematically forbidden for a single heavy quark. Therefore, in the frequency regime where gluodissociation dominates $\tilde{\kappa}$ is not the same as κ. However, in the static limit where dissociation via scattering (i.e., LD) is dominant, the two coefficients defined in Eqs. (19) and (22) seem identical, at the leading order. We have checked that the LD part of $\tilde{\kappa}$ agrees with the one obtained in Ref. [44].

We note that at higher order there is no reason for these two coefficients to be identical. The reason is that for quarkonium, chromoelectric field correlator is defined with Wilson lines in the adjoint representation [70]. On the other hand for a single heavy quark, Wilson lines are in fundamental representation.

It is useful to note here that in Eq. (22) if one makes $k_0, k \ll T$ approximation before integrating over k, the integrand is of the HTL form and is ultraviolet (UV) divergent. This is due to the fact that the applicability of the HTL resummation is restricted to the low-frequency limit. This divergence can be cured by either using a cutoff $k \approx m_D$ or by adding the UV contribution to the integral carefully [48]. However, the contribution from Eqs. (14) and (15) vanishes in the high-frequency limit. Therefore, if we use the imaginary part of the longitudinal self-energy given by Eqs. (7) and (8) and evaluate $\tilde{\kappa}$, the integral is convergent and can be computed numerically, which we do next.

In Fig. 2, we plot the electric field correlator arising from various contributions that appear in the evaluation of singlet self-energy diagram in Fig. 1 as a function of frequency. Here we take $T = 0.25$ GeV and Debye mass $m_D = 0.5$ GeV. The black curves are for the longitudinal gluon with a solid line for LD and a dashed one for pole contributions. The red curves are for transverse gluon where solid and dashed lines are for LD and pole contributions, respectively. As anticipated, in the small-frequency limit the dominant contribution comes from longitudinal gluon Landau damping. In this limit, other contributions are either zero or very small. Pole contributions switch on at a somewhat larger frequency, i.e., $k_0 \approx 0.2$ GeV. Moreover, the transverse gluon pole contribution is larger (in magnitude) compared to the longitudinal one. Finally, at high frequency, transverse pole contribution dominates and eventually approaches the corresponding free limit.

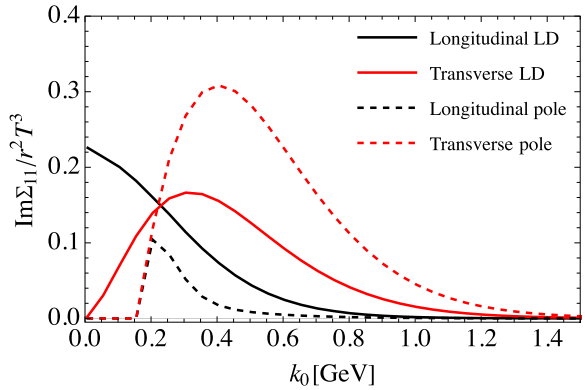

FIG. 2. Various contributions to scaled $\langle EE\rangle$ correlator as a function of frequency. Here we take $T = 0.25$ GeV and $m_D = 0.5$ GeV.

In Fig. 3, we have plotted $\tilde{\kappa}/T^3$ as a function of k_0. The red (dashed) curve here gets contribution from both $k_0 < k$ as well as $k_0 > k$ phase space regions. In the static limit, i.e., $k_0 \approx 0$, we have checked that $\tilde{\kappa}/T^3$ agrees with that in Ref. [44]. The black (solid) line is in the free limit, which, as expected, is zero at zero frequency.

It is well known that the perturbative result for κ is too low by roughly a factor of 5–10 than the nonperturbative value [69,71–74]. For example, recent lattice results for κ/T^3 are estimated as [72]

$$1.5 < \frac{\kappa}{T^3} < 2.8 \quad \text{for} \quad T = 1.5T_c,$$
$$0.9 < \frac{\kappa}{T^3} < 2.1 \quad \text{for} \quad T = 2.5T_c.$$

For finite k_0 there are no lattice results available in the literature. Naively, we expect them to be different from the perturbative estimates. Therefore, we expect that our predictions for R_{AA} are underestimated. However, our results capture the qualitative features of relative contributions of pole and LD in the range of temperatures available in HIC. Motivated by lattice QCD calculations of m_D, we choose $g = 2$ [42,58].

In the intermediate-frequency regime, the peak structure in $\tilde{\kappa}/T^3$ is from the transverse pole contribution. Finally, in the high-frequency limit, it merges with its free limit counterpart.

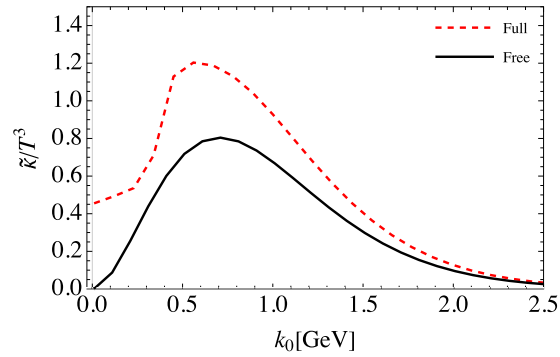

FIG. 3. $\tilde{\kappa}/T^3$ as a function of frequency for constant coupling $g = 2$, $T = 0.25$ GeV, and $N_f = 3$. Black (solid) line is the free limit and the dashed (red) is resummed one.

IV. DECAY WIDTH

At any given temperature T, the decay width of a singlet state $|\phi\rangle$ at leading order is given by

$$\Gamma = 2\,\langle\phi|\Im\Sigma_{11}|\phi\rangle, \tag{23}$$

where $\Im\Sigma_{11}$ is given in Eq. (3). Inserting a complete set of octet states $|o\rangle\langle o|$ at the right bracket of Eq. (3), one obtains

$$\begin{aligned}\Gamma &= 2\sum_o \langle\phi|r\hat{\mathcal{O}}(p_0,p,r)|o\rangle\langle o|r|\phi\rangle \\ &= 2\sum_o \mathcal{O}(p_0,p)\langle\phi|r|o\rangle\langle o|r|\phi\rangle,\end{aligned} \tag{24}$$

where summation is over all octet states allowed by the selection rule. In operator form $\mathcal{O}(p_0,p)$ is same as defined in Eq. (3) and now $p_0 = q_0 - k_0$ in terms of the chromoelectric spectral function as shown in Eq. (2).

Let us note that the EE correlator that enters in decay width is evaluated at frequency $k_0 = q_0 - p_0$. We remark here that the gluodissociation contribution to the dissociation rate in the hierarchy $E_b \gtrsim T$ has been written in terms of the chromoelectric field correlator, with the same frequency dependence also in Ref. [75,76]. Their formalism is applicable also for $E_b \sim T$ but the evaluation of the gluodissociation rate in Ref. [75,76] was done in the high-frequency limit by approximating the EE correlator by that of a noninteracting gluon gas. The gluodissociation contribution in the high-frequency limit for $T \sim E_b \gg m_D$ was computed in Ref. [47] and in this regime our expressions agree with theirs. Let us note that the octet state lies in the continuum. q_0 is the energy of the octet state, which is given by,

$$q_0|o\rangle = \left(V_o + \frac{\hat{q}^2}{M}\right)|o\rangle. \tag{25}$$

One point to note is that momentum conservation implies that the center-of-mass momentum of the octet state is $-k$. This implies that the energy of the $|o\rangle$ state has an additional contribution $k^2/(4M)$, which should be added to the right-hand side of Eq. (25). The value of k is governed by T since it is the region in k space where the gluon spectral function multiplied by the Bose-Einstein distribution function is not exponentially suppressed. In the hierarchy we are working, E_b and T are both small scales compared to M and hence quantities of the order of $T^2/(4M)$ are suppressed by an extra power of M compared to the right-hand side of Eq. (25) and hence can be safely dropped.

A. Modeling the singlet state

To complete the evaluation of Eq. (24), we need the functional form of the singlet state $|\phi\rangle$ as well as octet state $|o\rangle$. The final decay rates are sensitive to the choice of the wave functions. Various prescriptions have been used to model the wave functions in the thermal medium.

For a state created in vacuum and dropped into the QGP, a natural choice for $|\phi\rangle$ is the wave function in vacuum. Further, if the thermal effects are weak then $|o\rangle$ can be taken to as octet states in vacuum. If the initial formation of quarkonia is not affected by the medium (for example if the formation of the quarkonium states occurs on a time scale much shorter than the formation of the QGP) then this is a well-motivated model for $|\phi\rangle$ and $|o\rangle$. This picture has been previously used for phenomenology [36,77]. More formally, as discussed above, if we assume the hierarchy $1/r \gg T \sim E_b \sim m_D$ in pNRQCD, the real part of the potential at the scale E_b is the vacuum potential [46,48]. This is the Coulombic potential to the lowest order in α_s and the corresponding bound states are Coulombic bound states. This is one of the cases we consider below as described in Sec. IV A 2.

Another prescription common in the literature is the use of the eigenstates of the real thermal potentials corresponding to the instantaneous temperature during evolution [21,37]. This is one of the models we will consider in this paper and we describe it in Sec. IV A 1.

1. Eigenstates of instantaneous thermal potentials

At the LHC and the RHIC, the formation time of the QGP is a fraction of a fm/c and is not substantially larger than the formation time of quarkonia, of the order of $1/E_b$. One can expect the formation dynamics of quarkonia to be substantially affected by the medium.

One natural way to include these effects is to start the evolution from a narrow initial $Q\bar{Q}$ state of width $\approx M$ and follow its quantum evolution from very early time [40,42]. In this paper, we do not study the quantum dynamics and this analysis is beyond the scope of the paper. If dissociation can be modeled by the imaginary part of the potential (i.e., in the $E_b \ll T$ regime) another possible approach is to assume that the evolution dynamics is slow (adiabatic approximation) and the quarkonium state is initially formed in the eigenstate of the complex potential and at each instant the quarkonium state is in the eigenstate of the complex potential [27,28]. In this paper, dissociation is calculated using Eq. (3), which can not be captured by a complex potential and hence the adiabatic method is not applicable. We model the effect of the medium on the formation of quarkonia by making the maximal approximation that the initial state and subsequent to formation is determined by the real part of the instantaneous thermal potential [21,37].

More concretely, for the singlet states wave function, we use the eigenstates

$$p_0|\phi\rangle = \left(\frac{p^2}{M} + V_s(r,T)\right)|\phi\rangle, \tag{26}$$

where $V_s(r,T)$ is the real part of the thermal potential. Here we have subtracted the rest energy from all the $Q\bar{Q}$ states. Similarly, $|o\rangle$ is given by Eq. (25) with V_o given by the real part of the octet potential in the thermal medium. In summary, to calculate $|\phi\rangle$ and $|o\rangle$ we need the real parts of the potentials V_s, V_o.

For the singlet potential we use the lattice inspired potential, which is given by Refs. [42,78]

$$V_s(r,T) = -\frac{a}{r}(1+m_D r)e^{-m_D r} + \frac{2\sigma}{m_D}(1-e^{-m_D r}) - \sigma r e^{-m_D r}. \tag{27}$$

The effective coupling $a = 0.409$ and the string tension $\sigma = 0.21\ \mathrm{GeV}^2$ are fixed from the vacuum masses and binding

TABLE I. Binding energies, mass and $\langle r^2 \rangle$ of various bounds state at $T = 0$ using Eq. (27). All dimensions are in GeV.

	$\Upsilon(1S)$	$\Upsilon(2S)$	$\chi_b(1P)$	$\Upsilon(3S)$	$\chi_b(2P)$
M_M	9.46	10.0	9.88	10.36	10.25
E_b	1.20	0.66	0.78	0.30	0.41
$\langle r^2 \rangle$	1.42	6.58	4.20	13.68	10.60

energies (see Table I) with bottom mass $M = 4.7$ GeV [42]. Here we take $m_D = 0$ to obtain the vacuum spectrum.

For finite T we keep a and σ the same as in $T = 0$ and $m_D = \sqrt{(1 + N_f/6)}gT$. For $g = 2$ Eq. (27) gives potentials consistent with those used for bottomonium phenomenology with lattice-based potentials [31,59]. We have checked that the potentials agree with the real parts of the potentials extracted nonperturbatively on the lattice (Ref. [79]) within error bars. For comparison, we note that the potentials are very similar to the Set 2 considered in Ref. [45].

The $Q\bar{Q}$ potential in the medium is screened, as a result of which E_b becomes smaller with increasing temperature. At sufficiently high temperature the bound state is dissolved [3]. It is worth mentioning that for the 1S state, the wave function does not depend on the temperature of the medium up to $T \approx 480$ MeV and it remains approximately the same as that of vacuum Coulombic state while the excited states dissolve earlier [45].

In Fig. 4, we plot the binding energy of $\Upsilon(1S)$, $\Upsilon(2S)$, and $\Upsilon(3S)$ states as a function of medium temperature. At $T = 0$, E_b is given by

$$E_b = 2M - M_M + V_\infty, \tag{28}$$

where M is bottom current mass, M_M is bound state mass, and V_∞ is the asymptotic value of real part of the potential. For parameters in Table I, we use the potential given in Ref. [42]. Let us note that while $M_M - 2M$ is a small quantity the actual binding energy is not small because of the $V_\infty (\approx 1.2$ GeV). This phenomenological approach for obtaining the Υ spectrum reasonably describes the mass spectrum [42].

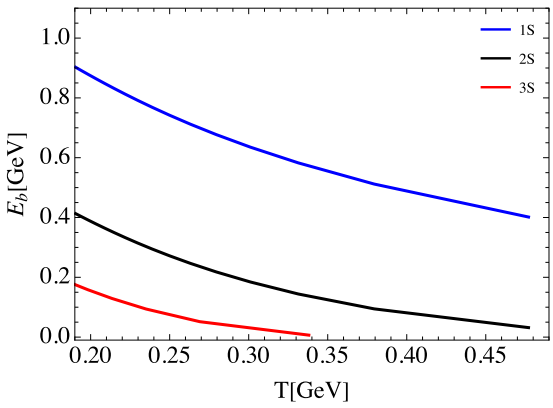

FIG. 4. Binding energies for $\Upsilon(1S)$, $\Upsilon(2S)$, and $\Upsilon(3S)$ states as a function of temperature. Here we take constant coupling $g = 2$.

Moreover, for finite T, we solve Eq. (26) and obtain E_b using

$$E_b(T) = V_\infty(T) - p_0(T). \tag{29}$$

The key point we want to highlight in Fig. 4 is that for the temperature range relevant for HICs, the hierarchies $E_b \gg T$ or $E_b \ll T$ may not be satisfied, at least for 1S and 2S states. It is worth mentioning that E_b obtained here agrees with the one in Ref. [80]. On the other hand for higher states, binding energy approaches zero around this temperature and $E_b \ll T$.

It is worth mentioning here that both the binding energy and heavy quark mass are scheme dependent [81]. This arises since the loop corrections in the heavy quark pole mass and the interaction potential have an infrared renormalon [82,83] and different prescriptions have been used in the literature [81,84,85] to define renormalon subtracted heavy quark masses. We leave a systematic analysis of the effect of the scheme dependence of the bottomonium mass on our results for future work. We only note here that the value of the bottom quark mass used in our calculations ($M = 4.7$ GeV) is within one standard deviation of the values obtained in Ref. [81] for the RS' scheme at the renormalization scale of 2 GeV. It is about 7% larger than the values obtained in Ref. [81] for a different (RS) scheme at the renormalization scale of 2 GeV.

A consequence of this model is that we can not address the observed phenomenology of the 3S state [86] as for the central bins R_{AA} for 3S state (in this model) is zero. The key dynamics missing from the classical model are (i) quantum formation dynamics and (ii) processes that allow for reformation of bound states, which are important for capturing 3S dynamics.

2. Eigenstates of Coulombic potentials

An alternative choice follows from pNRQCD [6,48] if we assume that the hierarchy $1/r \gg T$, m_D, $\Lambda_{\rm QCD}$ is very well satisfied. In that case the potential at the distance scale r is strictly unaffected by thermal and screening effects. Furthermore, assuming $1/r \gg \Lambda_{\rm QCD}$ (since T is comparable to $\Lambda_{\rm QCD}$ in the QGP), the potential at the distance scale r is also unaffected by nonperturbative effects. Therefore, in this regime

$$V_s(r, T) = -\frac{\xi}{r}. \tag{30}$$

Following Ref. [15] we take $M = 4.8$,

$$E_b(1S) = 0.47\,\text{GeV}. \tag{31}$$

For these parameters,

$$E_b(2S) = 0.12\,\text{GeV}, \tag{32}$$

and,

$$\xi = 0.62. \tag{33}$$

This is the second choice we will consider in our analysis.

B. Modeling the octet state

The octet states are also affected by the thermal medium. At short distances we know that the potential is repulsive

Coulombic. In perturbation theory both the real and the imaginary parts of the medium modified octet potential have been computed [52]. Recently, both the real and imaginary parts of the octet potential have also been computed in pure gluonic theory on the lattice [49]. An important outcome from these papers is that in both perturbative and nonperturbative calculations one finds that at large r the singlet potential approaches the octet potential. This is still an active area of research but the form of the potential for $2+1$ flavor QCD is not yet known.

Based on these considerations, we take two limiting cases for the octet potential. The first is when the screening is strong and one can ignore the octet repulsion at the distance scale of interest and hence

$$V_o(r,T) = V_\infty, \tag{34}$$

where $V_\infty = \frac{2\sigma}{m_D}$ is the asymptotic value of singlet potential. In this case, the $|o\rangle$ wave functions are the same as the wave functions of the free particle but the energy levels start from V_∞.

The other limit is where the screening is weak (gluodissociation in this case was discussed for Coulombic singlet states in Ref. [47]) and

$$V_o(r,T) \to C_F \frac{\alpha}{2Nr} + V_\infty. \tag{35}$$

We expect the true physics to be between these two limiting cases.

Finally, the octet potential also has an imaginary piece, which corresponds to the scattering of the octet state to the singlet state or an octet state. In this paper, we assume that these processes do not significantly regenerate bound states because the octet states are much broader than the singlet state. This is found to be phenomenologically important in quantum calculations for the excited $\Upsilon(2S)$ and $\Upsilon(3S)$ [73,87,88] but is ignored in our calculation.

For the repulsive Coulombic potential, the general form of the radial wave function is given as [89]

$$R_l(\rho) = \frac{C_l}{\rho}\rho^{l+1}e^{i\rho}{}_1F_1(1+l+i\nu, 2l+2, -2i\rho), \tag{36}$$

where ${}_1F_1$ is confluent hypergeometric function, $\rho = rp$, $\nu = \frac{1}{8a_0 p}$ with $a_0 = \frac{2}{\bar{\alpha}M}$ as Bohr radius. The normalization factor C_l in Eq. (36) reads as

$$C_l = \frac{2^l e^{-\frac{\nu\pi}{2}}\sqrt{\Gamma(1+l+i\nu)\Gamma(1+l-i\nu)}}{\Gamma(2+2l)}. \tag{37}$$

Let us note that for the above form of C_l, the wave function obeys the following form for normalization:

$$\int r^2 R_l(pr)R_l(p'r) = \frac{(2\pi)^3}{p^2}\delta(p-p'). \tag{38}$$

With this choice of normalisation, the decay width has the form given in Eqs. (42), (43), and (45). With the above form of the radial wave function, the general form of the octet wave function can be written as

$$|o\rangle = 4\pi R_l(pr)\sum_m Y_m^{*l}(\hat{r})Y_m^{*l}(\hat{p}). \tag{39}$$

Here Y_m^l is spherical harmonics. For the 1P state, replacing $l = 1$ in the obove equation and summing over quantum number m, the octet wave function $|o\rangle$ reads as

$$|o\rangle = \sqrt{2\pi}\mathbf{p}\cdot\mathbf{r}e^{ipr}\sqrt{\frac{\nu(\nu^2+1)}{e^{2\pi\nu}-1}}{}_1F_1(2+i\nu, 4, -2ipr). \tag{40}$$

For $s(d)$ states, the wave function can be obtained by replacing $l = 0(2)$ in Eq. (39).

In the case of no final-state interaction, we take free wave function, which in terms of Bessel function is given as

$$|o\rangle = 4\pi j_l(pr)\sum_m Y_m^{*l}(\hat{r})Y_m^l(\hat{p}). \tag{41}$$

Below we discuss the contribution from the Landau damping and gluon absorption in the decay width.

C. Landau damping contribution

One way to organize the kinematic regimes, which contribute to the decay width [Eq. (23)], is spacelike and timelike. Dissociation (of quarkonia) via scattering of the bound state with the thermal partons occurs when the momentum of the exchanged gluon is spacelike. As mentioned, this mechanism is known as LD. It is estimated by taking the resummed propagator for the gluon line in Fig. 1. The LD contribution is dominant when $E_b \ll m_D, T$ [6]. The overall contribution is both from the longitudinal as well as transverse gluon. Moreover, in the small k_0 limit, the longitudinal gluon contribution turns out to be dominant. This is easily understood by noting that while both ρ_L and ρ_T go as k_0 at small k_0, ρ_T is multiplied by $(k_0)^2$ in Eq. (3) while ρ_L is multiplied by $(k_i)^2$. For $E_b \ll m_D, T, k_0 \ll k$, and hence the longitudinal gluon contribution turns out to be dominant. However, we evaluate both of them numerically and do not drop the transverse contribution.

The explicit expression of the contribution to Γ_L from Eq. (7) in the numerator [gluon loop contribution to $\Im\Pi_L(k_0,k)$] by the transition from a specific $|\phi\rangle$ to a specific $|o\rangle$, is given [see Eq. (24)] by,

$$\begin{aligned}\Gamma_L = {}& \frac{C_F g^4 N}{6\pi}\int d^3p f(k_0)\int d^3k \frac{k\theta(k-k_0)}{(k^2+\Re\Pi_L)^2+\Im\Pi_L^2} \\ & \times \int_{\frac{k+k_0}{2}}^{\infty} dq\, q^2\left(2+\frac{k^4}{4q^4}-\frac{k^2}{q^2}\right)[f(q-k_0)-f(q)] \\ & \times |\langle\phi|r|o\rangle|^2.\end{aligned} \tag{42}$$

Here p is relative momentum between in the Q and $\bar{Q}$ in the octet state, defined by its energy from the threshold ($E_o = \frac{p^2}{M}$), and $k_0 = \frac{p^2}{M} - E$ where E is binding energy of the bound state.

For finite N_f (we will take $N_f = 3$ in our calculation), $\Re\Pi_L$ and $\Im\Pi_L$ get contributions from the gluon as well as quark loop. The quark loop contribution has $\Im\Pi_L$ with the form given in Eq. (8) and gives a similar expression to Eq. (42) that we do not write explicitly here. The total longitudinal contribution is obtained by adding the quark loop and the gluon loop contributions and summing over the final state $|o\rangle$ (really an integral over p). Assuming a strong hierarchy

between E_b and T, this can be simplified to the one obtained in Ref. [6].

The transverse gluon contribution arises from the transverse part of the spectral function given in Eq. (15). As may be noticed in Eq. (3), for finite k_0 this term can not be ignored. Moreover, at significantly large k_0, this term can dominate over the longitudinal gluon contribution. This situation may arise when the hierarchy between E_b and medium temperature is not very strong. This can be observed from Fig. 2 that for k_0 sufficiently large, the transverse contribution to $\Im\Sigma_{11}$ can be larger than the longitudinal. It is also clear that in the kinematic regime where the transverse LD contribution is comparable to the longitudinal LD contribution, the binding energy and the final-state interactions can not be ignored in either.

Following the similar prescription as for the case of longitudinal gluon, the contribution to the decay width from the transverse gluon from the gluon loop reads as

$$\Gamma_T = \frac{g^4 C_F N}{3\pi}\int d^3p f(k_0)\int d^3k \frac{k_0^2\theta(k-k_0)}{\left(k_0^2-k^2-\Re\Pi_T\right)^2+\Im\Pi_T^2} \times \frac{1}{k}\int_{\frac{k+k_0}{2}}^{\infty} dq\left(q^2\left(1-\frac{k^2}{2q^2}\right)^2-\frac{k^2}{4}\left(2-\frac{k^2}{2q^2}\right)^2\right) \times [f(q-k_0)-f(q)]|\langle\phi|r|o\rangle|^2. \tag{43}$$

The total contribution from Landau damping is sum of Eqs. (42) and (43).

D. Pole contribution

In the kinematic regime $E_b \gg T$, the dominant contribution to quarkonium dissociation from singlet to unbound octet state occurs by absorbing a timelike gluon from the thermal medium. This process is known as gluodissociation [47]. For the decay width evaluation, the contribution to the quarkonium self-energy arises from the pole of the gluon propagator. In the free limit, i.e., $T \gg E_b$, the medium contribution to the singlet to octet thermal breakup appears in the thermal weight only. However, in the intermediate temperature range, HTL effects also become important and one needs to use resummed propagator. In the HTL resummed propagator, both longitudinal and transverse gluon contribute to the imaginary part of the gluon propagator. After adding both of these contributions and performing k_0 integration using energy δ function, $\Im\Sigma_{11}$ reads as

$$\Im\Sigma_{11}^P = \frac{C_F g^2 r^2}{6} f(k_0)\int d^3k\left(\frac{2k_0^2\delta\left(k-k_0^T\right)}{|\partial\Re\Pi_L/\partial k|_{k_0^T}} + \frac{k^2\delta\left(k-k_0^L\right)}{|\partial\Re\Pi_T/\partial k|_{k_0^L}}\right), \tag{44}$$

where k_0^T is solution of $k_0^2-k^2-\Re\Pi_T=0$ and k_0^L is that of $k_0^2-\Re\Pi_L=0$. In the limit $T \gg E_b$, Eq. (44) can be solved analytically by making an expansion in the bosonic distribution and replacing the spectral function by the free spectral function. Using Eq. (44), decay width is given as

$$\Gamma_P = \frac{C_F g^2}{3}\int d^3p f(k_0)\int d^3k\left(\frac{2k_0^2\delta\left(k-k_0^T\right)}{|\partial\Re\Pi_T/\partial k|_{k_0^T}} + \frac{k^2\delta\left(k-k_0^L\right)}{|\partial\Re\Pi_L/\partial k|_{k_0^L}}\right)|\langle\phi|r|o\rangle|^2. \tag{45}$$

The contribution of transverse gluon to the decay width of the bound states is dominant over the longitudinal one. This can be observed from the frequency behavior of $\Im\Sigma_{11}$ shown in Fig. 2. Below we discuss the results obtained for the decay width and R_{AA}.

V. RESULTS FOR CLASSICAL DYNAMICS

In this section, we discuss the results for $\Upsilon(1S)$ and $\Upsilon(2S)$ states using the decay width obtained in the previous section. We mainly focus on the relative contributions of pole and LD within the perturbative limit and show the overall effect on R_{AA}.

At any given time t, the survival probability of a given singlet state can be obtained by using the rate equation

$$\frac{dN(t)}{dt} = -N(t)\sum_i \Gamma_i(t), \tag{46}$$

where $N(t)$ is the number of bound states at time t and summation is over the two contributions arising from LD and pole. The total number of states produced after some time t_f may be obtained from Eq. (46) and is given as

$$N = N_0 e^{-\int_{t_0}^{t_f}\Gamma(t)dt}. \tag{47}$$

Here t_0 is the initial time, N_0 is number of bound states at time t_0, and $\Gamma(t)=\sum_i\Gamma_i(t)$.

A. Medium model

To calculate Γ as a function of time we need a model for the background evolution of the thermal medium. In this paper we use a simple model and take the medium by a Bjorken expanding medium [90] with a temperature

$$T(t) = T(t_0)\left(\frac{t_0}{t}\right)^{\frac{1}{3}}. \tag{48}$$

We are interested in quarkonia with zero rapidity and hence have replaced the proper time with the local time. $T(t_0)$ is the temperature at a reference proper time t_0. We take $t_0 = 0.6$ fm, which is a little later than the start of hydrodynamics for LHC energies [91]. This is starting time for the quarkonium evolution and is comparable to the formation time for quarkonia. Similar numbers were taken in Ref. [41].

The temperature at time t_0 depends on the impact parameter or equivalently the centrality. We use centrality bins analogous to the one used in ALICE [92]. For this purpose, we use the Glauber model (we do not use the Monte Carlo Glauber model here though we see that the difference between our centrality bins and the bins obtained from the Monte Carlo Glauber model [93] is small) to relate the impact parameter

TABLE II. Mean value of $N_{\rm part}$, impact parameter (b) and initial temperature (T_0) for various centrality bins. T_0 is temperature at time $t_0 = 0.6$ fm. The left column in T_0 is for $f = 1.462$ and the right one is for $f = 1.782$ [see text below Eq. (53)].

Centrality (%)	Npart	b (fm)	T_0	(MeV)
0–2.5	393	2.5	446	478
2.5–5	363	3.5	443	475
5–7.5	334	5.0	439	470
7.5–10	307	7.0	434	465
10–20	248	8.7	420	450
20–30	173	10.0	408	437
30–40	116	11.2	371	398
40–50	74	12.2	317	339
50–60	44	13.2	267	286
60–70	23	14.0	207	222

to the number of participants ($N_{\rm part}$) and the number of binary collisions($N_{\rm bin}$). Following ALICE, bins in the observed $dN_{\rm ch}/d\eta$ are related to bins in $N_{\rm part}$ using the relation

$$\frac{dN_{\rm ch}}{d\eta} = \lambda[fN_{\rm bin} + (1-f)N_{\rm part}], \tag{49}$$

where $\lambda = 2.75$ and $f = 0.212$ [92]. With these values of the parameters λ and f, we quantitatively agree with the centrality dependence of $dN_{\rm ch}/d\eta$ as a function of $N_{\rm part}$ given in Fig. 10 of Ref. [94]. For each centrality bin, we have mentioned the mean value of $N_{\rm part}$ and impact parameter b in Table II.

With $dN_{\rm ch}/d\eta$ in hand for each centrality bin, the initial temperature at t_0 is obtained by using following prescription [95]. The value of $d\mathcal{N}/dy$ is related to the experimentally measured charged particle multiplicity by the relation,

$$\frac{d\mathcal{N}}{dy} = \frac{3J}{2}\frac{dN_{\rm ch}}{d\eta}, \tag{50}$$

where $J = 1.12$ is the Jacobian for y to η transformation [96]. $\mathcal{N}$ is the multiplicity of the particles produced at the end, y is pseudorapidity. The factor 3/2 in Eq. (50) incorporates the contribution from neutral particles. In order to be consistent within our model, for each centrality bin, we take $dN_{\rm ch}/d\eta$ obtained by using Eq. (49) with the parameters mentioned above.

In the nuclear collision experiments, the number density of partons or entropy is decided by the rapidity distribution of the produced particles. Assuming that initially the system is at chemical equilibrium, and assuming that the entropy does not change during the evolution, we can write the initial parton density as

$$n_0 = \frac{1}{A_\perp t_0}\frac{d\mathcal{N}}{dy}, \tag{51}$$

where $A_\perp$ is transverse size of the system. We estimate it from the Glauber model for each centrality via [97]

$$A_\perp = 4\pi\sqrt{\langle x^2\rangle\langle y^2\rangle}, \tag{52}$$

where $\langle x^2\rangle$, $\langle y^2\rangle$ is size along the transverse directions. A rough estimate of T_0 can be made from the initial number density assuming a noninteracting QGP. Then, $n_0 = (\beta_1 + 2\beta_2)T_0^3$ with $\beta_1 = 8\pi^2/15$ and $\beta_2 = 7\pi^2 N_f/40$ represents equilibrium density for gluon and quark. Plugging it back in Eq. (51) along with Eq. (50), we obtain the initial temperature at time t_0 to be

$$T_0 = \left(\frac{3J}{2A_\perp t_0}\frac{dN_{ch}}{d\eta}\frac{1}{\beta_1 + 2\beta_2}\right)^{\frac{1}{3}}. \tag{53}$$

For $\sqrt{s} = 2.76$ TeV, Eq. (53) gives $T_0 \approx 250$ MeV for the most central bin (0–2.5 %). This is significantly lower than estimates of the temperatures obtained at $t_0 \approx 0.6$ fm in hydrodynamic simulations [91]. We note that Eq. (51) ignores various effects such as particleization, viscous effects, interaction in the QGP, and expansion in the transverse direction. Moreover, losses in the work done by the system during the expansion are also not taken into account. These effects may lead to entropy generation and energy loss restricting the applicability of Bjorken expansion. Thus the initial parton density will be somewhat larger than estimated by Eq. (51). In order to take these losses into account we redefine the initial parton density by multiplying Eq. (51) with a fudge factor (f), i.e., $n_0 = fn_0$.

This fudge factor is adjusted in such a way that we obtain the initial temperature in the most central bin to range from $T_0 \approx 450$ MeV ($f = 1.46$) to $T_0 \approx 480$ MeV ($f = 1.78$) at $t_0 = 0.6$ fm. For our final results of R_{AA} we provide the band corresponding to these two values of the initial temperatures. While this is a highly simplified model for the background medium, we hope that this band of variation captures important features of its hydrodynamic evolution. In Fig. 5, we show the variation of temperature as a function of time starting with $t_0 = 0.6$ fm till the temperature reaches the final value of 190 MeV.

Finally, for completeness, we also consider the final state feed-down effect, we follow the prescription given in Ref. [42]. Therefore, for a given bound states, R_{AA} is given by

$$R_{AA} = \frac{N + \alpha N_h}{N_0 + \alpha N_{0h}}, \tag{54}$$

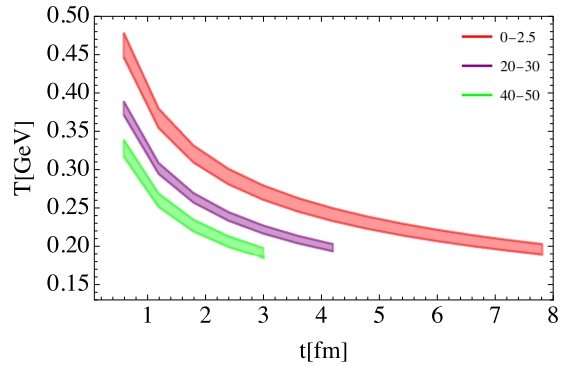

FIG. 5. Temperature as a function of time. Red band is for the most central bin and, central and green one are for 20–30 % and 40–50 % centrality, respectively. Here the initial time $t_0 = 0.6$ fm for all centrality bins. The band here covers upper and lower temperature corresponding to two different values of the fudge factor.

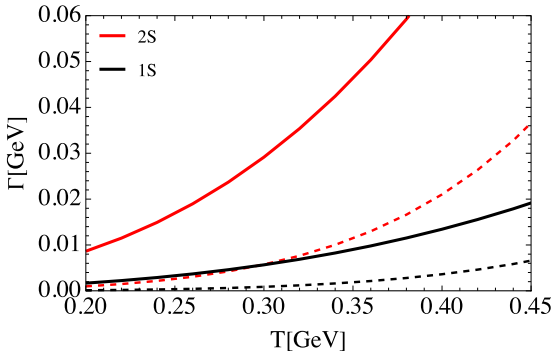

FIG. 6. Longitudinal LD contribution to the decay width of 1S (black) and 2S (red) states. The width obtained by using the imaginary potential (solid line) given by Eq. (55) is compared with the longitudinal LD contribution (dashed line) given by Eq. (42) for the thermal potentials [Eq. (27)]. In this plot the octet is assumed to be a interacting state [Eq. (40)].

where N_h is number of higher states at the end of evolution and α is feed-down parameter from higher state (N_h) to the state being considered. Feed-down matrix is given in Eq. (5.2) of Ref. [42]. N_0 is number of states at the initial time t_0. In the results presented here, for feed down, we only consider higher states with contributions more than 10%. Thus for $\Upsilon(1S)$, we take the contribution from $\Upsilon(2S)$, $\chi_{b0}(1P)$, $\chi_{b1}(1P)$, and $\chi_{b1}(2P)$ states. We follow the same for $\Upsilon(2S)$ state as well. For more details on feed down see Ref. [42].

Now we have all the pieces needed to compute the decay width and the suppression of bottomonia. We discuss results for these below.

B. Results for the decay width

For clarity, in this section, we will only show results for the thermal potentials [Eq. (27)]. We will make comments on how the results change if we take the singlet potential to be Coulombic [Eq. (30), Sec. IV A 2]. In particular, the analog of Fig. 6 for the Coulombic potential, comparing the decay width from the LD contribution with the decay width calculated using the imaginary potential, is shown in Appendix.

Let us first start by only considering only the LD contribution from the longitudinal modes. This is of interest as it is well known that in the static limit, this gives an imaginary potential [4,98]. The decay width for the imaginary potential is obtained from

$$\Gamma = 2\langle\phi|\Im V_s(r,T)|\phi\rangle, \tag{55}$$

where $\Im V_s$ is the imaginary part of the singlet potential. The form of the potential is given in Refs. [4,98].

In order to be consistent with the r^2 expansion in Eq. (1), we also make this approximation in the imaginary part of the potential. In this limit, the momentum integration in the potential becomes divergent, limiting its applicability in the small momentum ranges. We therefore put an upper cutoff m_D to get a finite result for $\Im V_s(r,T)$. The resulting form is

$$\Im V_s(r,T) = \frac{g^2 T C_F m_D^2 r^2 \pi}{3}\int_0^{\sim m_D}\frac{d^3k}{(2\pi)^2}\frac{k}{\left(m_D^2+k^2\right)^2}. \tag{56}$$

The cutoff $\sim m_D$ is motivated by the fact that the screened HTL propagator giving the integrand in Eq. (56) is not the valid at scales $k > m_D$. A more sophisticated approach is to use weakly coupled QCD to compute the UV completion of the contribution to $\Im V_s$ from scales $\sim T$ (e.g., see Refs. [6,44]). Numerically, the simple approximation Eq. (56) gives similar results. The decay width [using Eq. (55) with Eq. (56)] for $\Upsilon(1S)$ and $\Upsilon(2S)$ states are shown by the solid line in Fig. 6. In the same figure, we show the decay width obtained from Eq. (42) with $E_b = 0.6$ GeV (for 1S) and 0.2 GeV for 2S. As may be noticed, $\Im V_s(r,T)$ gives a larger decay width, which can be understood as follows.

Equation (55) assumes that the binding energy of the singlet state, and the octet state energy (q^2/M) of the quarkonium states is negligible compared to the temperature. This can be seen from Eq. (42). The energy δ function gives $k_0 = q^2/M - E_b$. Taking the limit $k_0 \to 0$ (static limit) in Eq. (42) is equivalent to calculating the decay rate by using Eq. (55) with Eq. (56). The main takeaway from Fig. 6 is that for realistic parameter values values, the $k_0 \to 0$ approximation significantly overpredicts the decay rate from the longitudinal LD process.

We also remark that if we take the static limit and do not make a quadratic expansion in r in the imaginary potential [4,98], the decay width turns out to be even larger than that obtained using Eq. (56). This is because for the typical size of the lowest Υ states Eq. (56) is smaller than the full expression [4,98], although at large r Eq. (56) is larger.

Finally, we note that we obtain a qualitatively similar behavior if we use Coulombic states with binding energies given in Eqs. (31) and (32). The decay rate using the imaginary potential significantly overpredicts the actual LD contribution. This is because, while the binding energy for the Coulombic potential *is* somewhat smaller for Coulombic potential compared to the thermal potential, $E_b \ll T$ is still not a good approximation for the eigenstates of the Coulombic potential, and hence dynamic effects are important. For more details see Appendix. We comment that a similar reduction in the longitudinal LD contribution at finite k^0 was noticed in Ref. [12].

Now we consider all the contributions to the decay width [Eq. (24)]. Focussing on the thermal potentials [Eq. (27)], in Fig. 7 we plot the LD (longitudinal and transverse combined) and the pole (longitudinal and transverse combined) contributions to $\Upsilon(1S)$ state. For $\Upsilon(2S)$ we plot the same quantity in Fig. 8. The bands correspond to the effect of taking the no screening [Eq. (39)] and complete screening [Eq. (41)] scenarios. Here we take $E_b = 0.6$ GeV (for 1S) and $E_b = 0.2$ GeV (for 2S), which lie in the middle (see Fig. 4) of the binding energies within the temperature range of interest.

It may be observed (from Fig. 4) that the hierarchies $E_b \gg T$ or $E_b \ll T$ are not very well satisfied for both 1S and 2S states. One would therefore expect a significant contribution from the finite frequency region of Fig. 3. For $\Upsilon(1S)$, this may be observed in Fig. 7. As anticipated, with this value of E_b, pole (blue band) and LD (red band) give somewhat similar contributions for a wide range of temperatures.

Moreover, LD contribution dominates at high temperatures. Similarly, for $\Upsilon(2S)$ state, pole contribution is a bit larger at temperature $\approx$0.2 GeV and at high temperature, $\approx$0.4

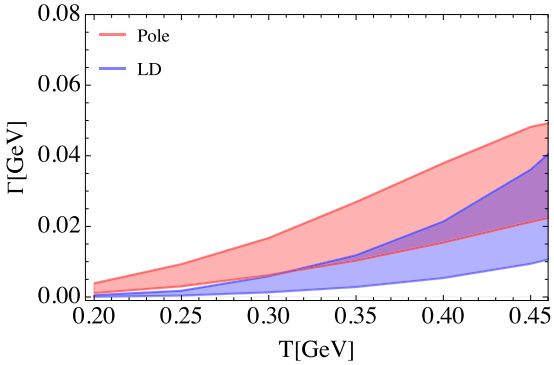

FIG. 7. All contributions to the decay width of the $\Upsilon(1S)$ state as a function of medium temperature. The upper curve of each band corresponds to the taking the octet states as free wave functions [Eq. (41)] and the lower curve of each band corresponds to taking the octet states as Coloumbic repulsive wave functions [Eq. (39)]. The red color band is the total LD contribution and the blue color band is the total pole (gluodissociation) contribution.

GeV, LD contribution is significantly larger than the pole contribution. This suggests that for $\Upsilon(2S)$ dissociation, LD gives the dominant contribution.

We have checked that this observation remains the same if we take Coulombic wave function for singlet- and final-state interactions in the octet channel. However, because of the smaller binding energy of Coulombic potentials, the transition from between pole and LD occurs at somewhat lower temperatures. This check is done with $E_b = 0.47$ GeV, for 1S. Similarly, for 2S, Coulombic states with $E_b = 0.12$ GeV, we find that this result does not change and LD remains the dominant contribution.

C. Results for R_{AA}

In Figs. 9 and 10, we combine both gluon absorption and scattering processes and plot R_{AA} for $\Upsilon(1S)$ and $\Upsilon(2S)$ state as a function of $\langle N_{\rm part}\rangle$ for each centrality bin. For a given centrality, we first evaluate singlet-state wave functions at each temperature by solving the Schrodinger equation given in Eq. (26). With temperature-dependent wave functions at hand, we estimate matrix element, i.e., $|\langle\phi|r|o\rangle|^2$

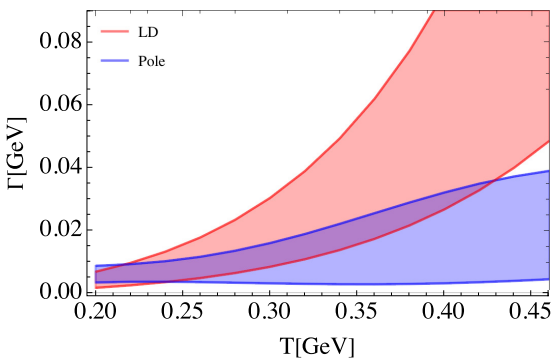

FIG. 8. Decay width of the $\Upsilon(2S)$ state as a function of medium temperature. The color conventions are the same as in Fig. 7

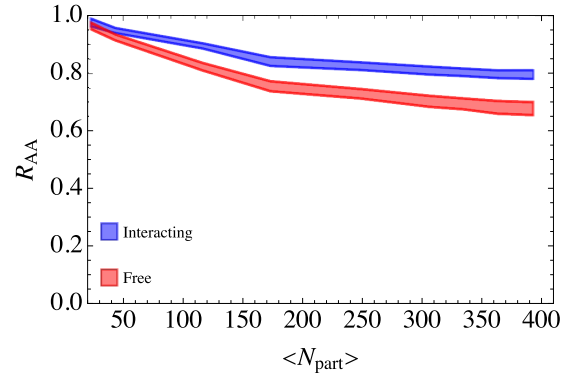

FIG. 9. R_{AA} for $\Upsilon(1S)$ state as a function of $\langle N_{\rm part}\rangle$ for each centrality bin. For blue color we take octet potential as vacuum potential and for red color we switch off octet potential assuming complete screening.

[see Eq. (42)] and obtain corresponding decay width for all processes. Here we use temperature-dependent binding energy shown in Fig. 4. Finally, we use Eq. (54) to estimate R_{AA} for a given state. As mentioned earlier, we consider two cases; (i) when there is no screening in the final-state octet interaction (shown in blue color) and (ii) when octet states are completely screened (shown in red color). Here, the upper and lower edge of the band corresponds to the lower and higher initial temperature given in Table II.

Let us note that in realistic situations, the octet potential is neither completely screened nor has the form of pure vacuum potential. Therefore, we expect the true value of suppression to lie somewhere between the blue and the red bands. It is evident that the suppression is underpredicted for these states. This may largely be due to the fact that the spectral functions are obtained at the leading-order (LO) accuracy. Further improvements of our results require nonperturbative estimate of these spectral functions on the lattice, which, so far, has been computed only in the static limit.

VI. CONCLUSION

In this work, we perform a comprehensive analysis to quantify the relative contributions arising from LD and gluodissociation to the $\Upsilon(1S)$ and $\Upsilon(2S)$ states within

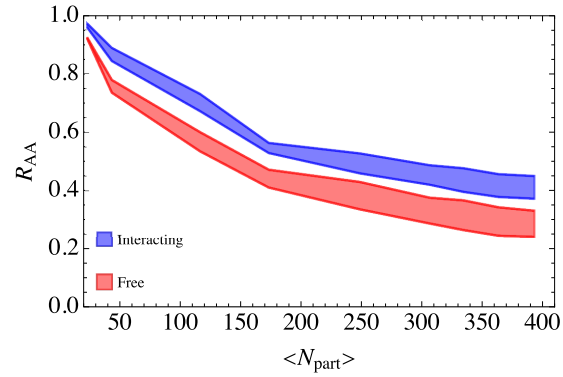

FIG. 10. R_{AA} for $\Upsilon(2S)$ state as a function of $< N_{\rm part} >$ for each centrality bin. Color representation is same as Fig. 9.

leading-order perturbation theory for the medium. We assume that the real part of the singlet potential is screened in a thermal medium, and we take lattice motivated real parts of the $Q\bar{Q}$ potential and estimate the binding energy and wave function as a function of T for Υ and χ states. By comparing the binding energy (shown in Fig. 4) and temperature it can be seen that for the 1S and 2S states both E_b and T are comparable to each other (although for the 2S state for $T >$ 300 MeV one could take $T \gg E_b$). We, therefore, expect that neither $E_b \gg T$ nor $E_b \ll T$ hierarchy is strictly satisfied in the interesting range of temperatures for the QGP, at least for 1S and 2S. However, for other higher excited states, $E_b \ll T$ seems to be satisfied quite well. For $\Upsilon(3S)$ this can be seen in Fig. 4.

We note that this conclusion does depend on the choice of the potential used to calculate the binding energy. For our analysis we have used lattice-motivated in-medium potentials [31,78]. It is possible that for weaker model potentials E_b will be smaller and the hierarchy $E_b \ll T$ might be a better approximation. It is interesting to note that even for the comparatively less binding Coulombic potentials (Appendix) we find that for $\Upsilon(1S)$, E_b is competitive with T, which has interesting consequences.

The consequence for the 1S state (and for the 2S in the later stages of the evolution) is that LD can not adequately describe the decay of the state. It is well known that in the static limit, i.e., $k_0 \to 0$, decay dominantly happens via longitudinal LD, which can be captured by an imaginary potential between $Q\bar{Q}$. However, this limit is valid if the binding energy of the quarkonium species is negligible compared to the medium temperature. As discussed in the text below Fig. 6, this also requires the kinetic energy of the octet states to be small. For $E_b \approx T$, the full finite frequency region of the spectral function for the chromoelectric field correlator becomes important. Let us note that Eq. (2) is valid in the case where thermal effects on the potential are small perturbations over vacuum potential. Therefore the eigenstates of the thermal Hamiltonian should be approximately the same as that of vacuum. This is indeed true for 1S state when $T < 500$ MeV. This is clear from the comparison of the total decay width computed using the eigenstates of the thermal potentials and the Coulomb potential shown in Fig. 12 in Appendix. For 2S state we do see a difference in the decay widths calculated using the thermal and the Coulombic potentials (Fig. 13 in Appendix), suggesting that the dipole approximation is being stretched to the limit of its applicability. Moreover, for higher states including 3S, this may not be applicable above T_c.

There is a caveat to the above conclusion. The perturbative value of the $k_0 \to 0$ value of the chromoelectric spectral function is a factor of 5–10 times smaller than the nonperturbative value calculated on the lattice. If this enhancement persists till k_0 values of a few 100 MeV (see Fig. 3) then our conclusion about the relative contribution of the LD and the other contributions will still be true. However, if the spectral function rapidly drops down towards the perturbative estimate (at $k_0 \approx$ GeV we expect the leading-order perturbative result to be more reliable) then the LD contribution dominates for all the states and the static results can be used to capture the physics of interest. This provides a motivation to study the spectral function at finite frequency nonperturbatively, although it is a difficult problem.

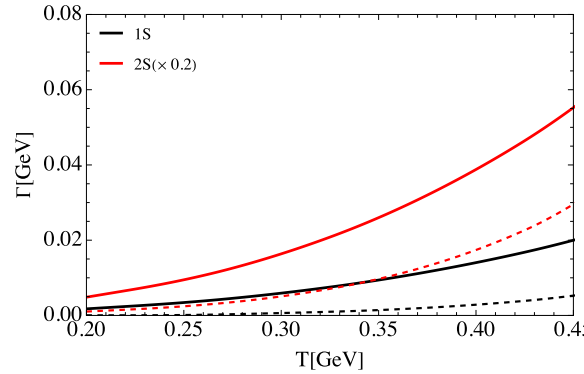

FIG. 11. Decay width of 1S (black) and 2S (red) from imaginary potential (solid line) and longitudinal LD (dashed line) using Coulombic wave functions both for 1S and 2S states.

The hierarchy between E_b and T (T is related to the inverse of the environment time scale) plays an important role while performing quantum calculations of quarkonia dynamics within the open quantum system framework. It has been shown [40,99,100] that if $E_b \ll T$ quarkonium system is in the quantum Brownian motion regime and the evolution is local in time. In this case, one can obtain a Lindblad equation for the density matrix evolution for the $Q\bar{Q}$ system. On the other hand if $E_b \gtrsim T$ then this proof fails. We show here that this is the case for the $\Upsilon(1S)$ state throughout the evolution if one considers the state to be an eigenstate of the instantaneous (real) potential. E_b is $\lesssim T$ for the excited states in the early part of the evolution. However, If substantial regeneration of the excited states happens at a later time (low temperature) then the hierarchy $E_b \gtrsim T$ might be satisfied. In this regime, if a quantum Brownian description of the dynamics is attempted, one might need dynamics that are correlated in time. Although a quantum optical description might become applicable in this case [75,76]. We do not discuss quantum evolution in this work and leave this for the future.

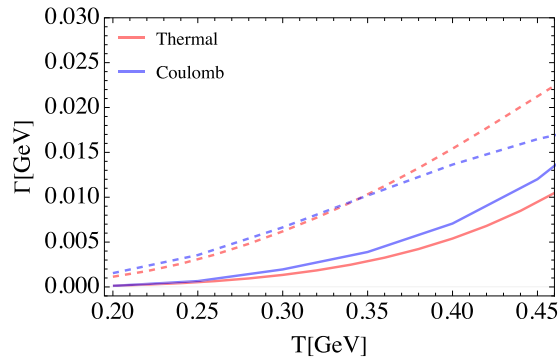

FIG. 12. Decay width of $\Upsilon(1S)$ for Coulombic wave function (blue) and temperature-dependent wave function (red). The dashed lines are pole contribution and solid line are Landau damping contribution to the decay width.

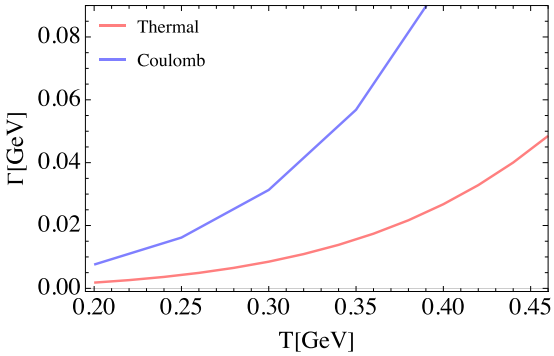

FIG. 13. The Landau damping contribution to the decay width of $\Upsilon(2S)$ for Coulombic wave function (blue) and temperature-dependent wave function (red). For the 2S the gluodissociation contribution is relatively much smaller and hence is not shown here.

ACKNOWLEDGMENTS

We acknowledge the support of the Department of Atomic Energy, Government of India, under Project Identification No. RTI 4002. We also thank N. Brambilla, S. Datta, and M. Strickland for valuable discussions.

APPENDIX: COULOMBIC WAVE FUNCTION

In Fig. 11, we show the decay width for 1S and 2S states using the Coulombic wave functions. For better visibility, we have scaled 2S decay width by a factor of 0.2. The corresponding binding energies of these states are given in Eqs. (31) and (32). Note that similar to the case of wave functions obtained using Eq. (26), for Coulombic states also, keeping the finite-energy transitions reduces the decay width.

For a clearer comparison, in Fig. 12, we show the decay width of $\Upsilon(1S)$ state for both Coulombic wave function (blue) with parameters discussed in Sec. IV A 2 and thermal wave function in red, with parameters discussed in Sec. IV A 1. We can see that for $\Upsilon(1S)$, temperature effects are small and hence can be treated as a perturbation. This is mainly because of the small size of $\Upsilon(1S)$ state, which satisfies pNRQCD hierarchies. Hence, the thermal potential seems to have a minor effect on the result.

On the other hand, $\Upsilon(2S)$ has a larger size and one can see that the results for the Coulombic and the thermal potentials differ (see Fig. 13). This suggests that the effects beyond the dipole approximation might be important for the 2S state.

[1] N. Brambilla, A. Pineda, J. Soto, and A. Vairo, Nucl. Phys. B **566**, 275 (2000).
[2] A. Pineda and J. Soto, Nucl. Phys. B **64**, 428 (1998).
[3] T. Matsui and H. Satz, Phys. Lett. B **178**, 416 (1986).
[4] M. Laine, O. Philipsen, M. Tassler, and P. Romatschke, J. High Energy Phys. 03 (2007) 054.
[5] G. Bhanot and M. E. Peskin, Nucl. Phys. B **156**, 391 (1979).
[6] N. Brambilla, J. Ghiglieri, A. Vairo, and P. Petreczky, Phys. Rev. D **78**, 014017 (2008).
[7] M. E. Peskin, Nucl. Phys. B **156**, 365 (1979).
[8] E. Braaten and R. D. Pisarski, Phys. Rev. D **42**, 2156 (1990).
[9] O. Kaczmarek, S. Ejiri, F. Karsch, E. Laermann, and F. Zantow, *Finite density QCD. Proceedings, International Workshop, Nara, Japan*, July 10–12, 2003; Prog. Theor. Phys. Suppl. **153**, 287 (2004).
[10] N. Brambilla, M. A. Escobedo, M. Strickland, A. Vairo, P. Vander Griend, and J. H. Weber, J. High Energy Phys. 05 (2021) 136.
[11] S. Caron-Huot and G. D. Moore, Phys. Rev. Lett. **100**, 052301 (2008).
[12] J.-P. Blaizot and M. A. Escobedo, Phys. Rev. D **104**, 054034 (2021).
[13] J.-P. Blaizot and M. A. Escobedo, Phys. Rev. D **98**, 074007 (2018).
[14] J.-P. Blaizot and M. A. Escobedo, J. High Energy Phys. 06 (2018) 034.
[15] N. Brambilla, M. A. Escobedo, A. Islam, M. Strickland, A. Tiwari, A. Vairo, and P. Vander Griend, J. High Energy Phys. 08 (2022) 303.
[16] A. Andronic *et al.*, Eur. Phys. J. C **76**, 107 (2016).
[17] L. Grandchamp, R. Rapp, and G. E. Brown, Phys. Rev. Lett. **92**, 212301 (2004).
[18] R. Rapp and H. van Hees, Heavy quarks in the quark-gluon plasma, *Quark-Gluon Plasma 4* (2010), pp. 111-206.
[19] X. Zhao and R. Rapp, Nucl. Phys. A **859**, 114 (2011).
[20] A. Emerick, X. Zhao, and R. Rapp, Eur. Phys. J. A **48**, 72 (2012).
[21] X. Zhao, A. Emerick, and R. Rapp, Nucl. Phys. A **904–905**, 611c (2013).
[22] X. Du, M. He, and R. Rapp, Phys. Rev. C **96**, 054901 (2017).
[23] X. Du and R. Rapp, J. High Energy Phys. 03 (2019) 015.
[24] F. Brezinski and G. Wolschin, Phys. Lett. B **707**, 534 (2012).
[25] F. Nendzig and G. Wolschin, Phys. Rev. C **87**, 024911 (2013).
[26] J. Hong and H. Su Lee, Phys. Lett. B **801**, 135147 (2020).
[27] M. Strickland, Phys. Rev. Lett. **107**, 132301 (2011).
[28] M. Strickland and D. Bazow, Nucl. Phys. A **879**, 25 (2012).
[29] M. Margotta, K. McCarty, C. McGahan, M. Strickland, and D. Yager-Elorriaga, Phys. Rev. D **83**, 105019 (2011); **84**, 069902(E) (2011).
[30] B. Krouppa, R. Ryblewski, and M. Strickland, Phys. Rev. C **92**, 061901(R) (2015).
[31] B. Krouppa, A. Rothkopf, and M. Strickland, Phys. Rev. D **97**, 016017 (2018).
[32] B. Krouppa, A. Rothkopf, and M. Strickland, Nucl. Phys. A **982**, 727 (2019).
[33] R. Katz and P. B. Gossiaux, Ann. Phys. (NY) **368**, 267 (2016).
[34] P. B. Gossiaux and R. Katz, Nucl. Phys. A **956**, 737 (2016).
[35] P. B. Gossiaux and R. Katz, J. Phys.: Conf. Ser. **779**, 012041 (2017).
[36] R. Sharma and I. Vitev, Phys. Rev. C **87**, 044905 (2013).
[37] S. Aronson, E. Borras, B. Odegard, R. Sharma, and I. Vitev, Phys. Lett. B **778**, 384 (2018).
[38] Y. Makris and I. Vitev, J. High Energ. Phys. 10 (2019) 111.
[39] S. Kajimoto, Y. Akamatsu, M. Asakawa, and A. Rothkopf, Phys. Rev. D **97**, 014003 (2018).
[40] N. Brambilla, M. A. Escobedo, J. Soto, and A. Vairo, Phys. Rev. D **96**, 034021 (2017).

[41] N. Brambilla, M. A. Escobedo, J. Soto, and A. Vairo, Phys. Rev. D **97**, 074009 (2018).
[42] A. Islam and M. Strickland, J. High Energy Phys. 03 (2020) 235.
[43] R. Sharma and A. Tiwari, Phys. Rev. D **101**, 074004 (2020).
[44] G. D. Moore and D. Teaney, Phys. Rev. C **71**, 064904 (2005).
[45] A. Mocsy and P. Petreczky, Phys. Rev. Lett. **99**, 211602 (2007).
[46] N. Brambilla, M. Á. Escobedo, J. Ghiglieri, J. Soto, and A. Vairo, J. High Energy Phys. 09 (2010) 038.
[47] N. Brambilla, M. Á. Escobedo, J. Ghiglieri, and A. Vairo, J. High Energy Phys. 12 (2011) 116.
[48] N. Brambilla, M. A. Escobedo, J. Ghiglieri, and A. Vairo, J. High Energy Phys. 05 (2013) 130.
[49] D. Bala and S. Datta, Phys. Rev. D **103**, 014512 (2021).
[50] G. T. Bodwin, E. Braaten, and G. P. Lepage, Phys. Rev. D **51**, 1125 (1995); **55**, 5853(E) (1997).
[51] M. A. Escobedo, J. Soto, and M. Mannarelli, Phys. Rev. D **84**, 016008 (2011).
[52] Y. Akamatsu, Phys. Rev. D **87**, 045016 (2013).
[53] A. Rothkopf, T. Hatsuda, and S. Sasaki, Phys. Rev. Lett. **108**, 162001 (2012).
[54] Y. Burnier, O. Kaczmarek, and A. Rothkopf, Phys. Rev. Lett. **114**, 082001 (2015).
[55] P. Petreczky, J. Phys. G: Nucl. Part. Phys. **39**, 093002 (2012).
[56] D. Bala and S. Datta, Phys. Rev. D **101**, 034507 (2020).
[57] D. Bala, O. Kaczmarek, R. Larsen, S. Mukherjee, G. Parkar, P. Petreczky, A. Rothkopf, and J. H. Weber (HotQCD), Phys. Rev. D **105**, 054513 (2022).
[58] O. Kaczmarek and F. Zantow, Phys. Rev. D **71**, 114510 (2005).
[59] Y. Burnier and A. Rothkopf, Phys. Rev. D **95**, 054511 (2017).
[60] P. Petreczky, A. Rothkopf, and J. Weber, Nucl. Phys. A **982**, 735 (2019).
[61] G. Parkar, O. Kaczmarek, R. Larsen, S. Mukherjee, P. Petreczky, A. Rothkopf, and J. H. Weber, PoS **LATTICE2022**, 188 (2023).
[62] T. Miura, Y. Akamatsu, M. Asakawa, and A. Rothkopf, Phys. Rev. D **101**, 034011 (2020).
[63] R. Kobes, Phys. Rev. D **43**, 1269 (1991).
[64] R. L. Kobes and G. W. Semenoff, Nucl. Phys. B **272**, 329 (1986).
[65] J. I. Kapusta and C. Gale, *Finite-Temperature Field Theory: Principles and Applications*, 2nd ed., Cambridge Monographs on Mathematical Physics (Cambridge University Press, Cambridge, 2006).
[66] M. L. Bellac, *Thermal Field Theory*, Cambridge Monographs on Mathematical Physics (Cambridge University Press, Cambridge, 2011).
[67] J. Casalderrey-Solana and D. Teaney, Phys. Rev. D **74**, 085012 (2006).
[68] C. H. Simon and G. D. Moore, J. High Energy Phys. 02 (2008) 081.
[69] A. Francis, O. Kaczmarek, M. Laine, T. Neuhaus, and H. Ohno, Phys. Rev. D **92**, 116003 (2015).
[70] A. M. Eller, J. Ghiglieri, and G. D. Moore, Phys. Rev. D **99**, 094042 (2019); **102**, 039901(E) (2020).
[71] D. Banerjee, S. Datta, R. Gavai, and P. Majumdar, Phys. Rev. D **85**, 014510 (2012).
[72] D. Banerjee, R. Gavai, S. Datta, and P. Majumdar, Nucl. Phys. A **1038**, 122721 (2023).
[73] N. Brambilla, V. Leino, J. Mayer-Steudte, and P. Petreczky (TUMQCD), Phys. Rev. D **107**, 054508 (2023).
[74] N. Brambilla, V. Leino, P. Petreczky, and A. vairo (TUMQCD), in *37th International Symposium on Lattice Field Theory (Lattice 2019) Wuhan, Hubei, China*, June 16–22, 2019 (2019).
[75] X. Yao and T. Mehen, Phys. Rev. D **99**, 096028 (2019).
[76] X. Yao and T. Mehen, J. High Energy Phys. 02 (2021) 062.
[77] Y. Park, K.-I. Kim, T. Song, S. H. Lee, and C.-Y. Wong, Phys. Rev. C **76**, 044907 (2007).
[78] A. Dumitru, Y. Guo, A. Mocsy, and M. Strickland, Phys. Rev. D **79**, 054019 (2009).
[79] D. Lafferty and A. Rothkopf, Phys. Rev. D **101**, 056010 (2020).
[80] X. Du, M. He, and R. Rapp, Nucl. Phys. A **967**, 904 (2017).
[81] C. Peset, A. Pineda, and J. Segovia, J. High Energy Phys. 09 (2018) 167.
[82] A. H. Hoang, M. C. Smith, T. Stelzer, and S. Willenbrock, Phys. Rev. D **59**, 114014 (1999).
[83] M. Beneke, Phys. Lett. B **434**, 115 (1998).
[84] A. Pineda, J. High Energy Phys. 06 (2001) 022.
[85] C. Ayala, G. Cvetič, and A. Pineda, J. High Energy Phys. 09 (2014) 045.
[86] CMS, Observation of the Υ(3S) meson and sequential suppression of Υ states in PbPb collisions at $\sqrt{s_{NN}} = 5.02$TeV, CMS-PAS-HIN-21-007 (2022).
[87] X. Yao, W. Ke, Y. Xu, S. A. Bass, and B. Müller, J. High Energy Phys. 01 (2021) 046.
[88] N. Brambilla, M. A. Escobedo, A. Islam, M. Strickland, A. Tiwari, A. Vairo, and P. Vander Griend, Phys. Rev. D **108**, L011502 (2023).
[89] M. Abramowitz and I. A. Stegun, *Handbook of Mathematical Functions with Formulas, Graphs, and Mathematical Tables*, 9th Dover printing, 10th GPO printing ed. (Dover, New York, 1964).
[90] J. D. Bjorken, Phys. Rev. D **27**, 140 (1983).
[91] N.-B. Chang *et al.*, Sci. China Phys. Mech. Astron. **59**, 621001 (2016).
[92] J. Adam *et al.* (ALICE), Phys. Rev. Lett. **116**, 222302 (2016).
[93] M. L. Miller, K. Reygers, S. J. Sanders, and P. Steinberg, Annu. Rev. Nucl. Part. Sci. **57**, 205 (2007).
[94] B. Abelev *et al.* (ALICE), Phys. Rev. C **88**, 044909 (2013).
[95] D. K. Srivastava, R. Chatterjee, and M. G. Mustafa, J. Phys. G **45**, 015103 (2018).
[96] J. Adam *et al.* (ALICE), Phys. Rev. C **94**, 034903 (2016).
[97] G. K. Eyyubova, V. L. Korotkikh, A. M. Snigirev, and E. E. Zabrodin, J. Phys. G **48**, 095101 (2021).
[98] M. Laine, O. Philipsen, and M. Tassler, J. High Energy Phys. 09 (2007) 066.
[99] Y. Akamatsu, Phys. Rev. D **91**, 056002 (2015).
[100] Y. Akamatsu, Prog. Part. Nucl. Phys. **123**, 103932 (2022).